Subdivision Surfaces for Electromagnetic Integral Equations

D. Dault†, J. Li†, B. Liu*, R. Zhao*, Y. Tong*, B. Shanker†
†Dept. Electrical and Computer Engineering, *Dept. Computer Science and Engineering
Michigan State University, East Lansing, MI

***Abstract*—Subdivision surfaces are a powerful geometrical modeling tool that has been used extensively in computer graphics. In this paper we develop a general subdivision-based basis scheme that can be applied to a wide range of electromagnetic integral equations, and demonstrate several features and advantages.**

I. Introduction

Subdivision surfaces are widely used in the computer graphics community to construct globally smooth, intrinsically refinable surfaces, e.g. for character animation (Pixar's *Toy Story 2*, *Cars*, etc.). For boundary integral equations, subdivision surfaces provide an efficient means for constructing higher order surfaces directly from low order meshes without requiring additional interpolation points; furthermore, the surface is globally smooth to second order everywhere but a small number of vertices, where it is first-order smooth. Subdivision surfaces can easily handle topologically complex geometries, can be easily deformed, and can also model sharp (discontinuous) features where desired. Subdivision has been used in thin-shell deformation problems (e.g. [1]), but to the authors knowledge has never been employed for electromagnetic boundary integral equations.

II. Loop Subdivision Surfaces

We focus on the Loop subdivision scheme [2] for triangular meshes; other element types may also be treated. Loop subdivision surfaces are defined through recursive refinement of an initial first order "primal" mesh, with the refinement rule used around a vertex $\mathbf{v}_i$ based on the "valence" N of the vertex, defined as the number of vertices that are connected to $\mathbf{v}_i$. Practical meshes contain a mixture of "regular" vertices ($N = 6$), and a small number of "irregular" vertices ($N \neq 6$).

Subdivision of a level k mesh to a level $k+1$ mesh about a vertex $\mathbf{v}_0^k$ proceeds by inserting one new vertex on each edge incident on $\mathbf{v}_0$ and recomputing the vertex positions, with the new level k vertex positions given by

$$\mathbf{v}_i^{k+1} = (3\mathbf{v}_0^k + \mathbf{v}_{i-1}^k + 3\mathbf{v}_i^k + \mathbf{v}_{i+1}^k)/8 \qquad (1)$$

for the new vertices, and

$$\mathbf{v}_0^{k+1} = (1 - Nw)\mathbf{v}_0^k + w\mathbf{v}_1^k + \cdots + w\mathbf{v}_1^k \qquad (2)$$

for vertex $\mathbf{v}_0^k$, where $w = (10 - (3/2 + \cos(2\pi/N))^2)/(16N)$. Figure 1 shows a coarse sphere primal mesh, two refinements, and the limit surface ($k \to \infty$). Fortunately, the limit surface can be computed directly without infinite recursion. For triangles with three regular vertices, the limit surface is given by:

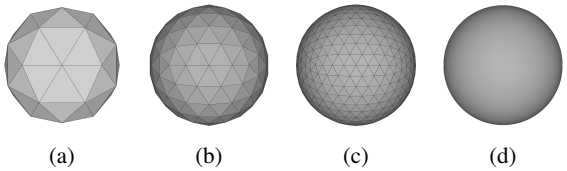

Fig. 1: Subdivision of a spherical mesh. (a) Primal mesh, (b) $k = 1$, (c) $k = 2$, (d) limit surface ($k = \infty$).

$$\mathbf{S}(\xi_1, \xi_2) = \sum_{i=1}^{12} N_i(\xi_1, \xi_2)\mathbf{v}_i, \qquad (3)$$

with ξ_1, ξ_2 the independent barycentric coordinates, $N(\xi_1, \xi_2)$ twelve quartic box splines tabulated in [3], and $\mathbf{v}_i$ the vertices in the triangle's neighborhood. Fig. 2 shows the neighborhood of a triangle T_l with two regular vertices and one valence N irregular vertex. Evaluation of the limit surface around irregular vertices uses a modified form of (3) [3].

III. Subdivision for Electromagnetic BIEs

Given that the limit surface may be expressed analytically as (3), the local tangent vectors may be obtained

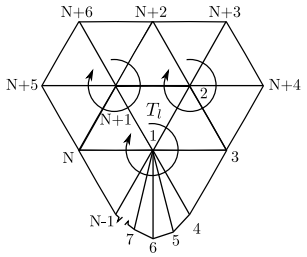

Fig. 2: Neighborhood of triangle T_l. Vertex $\mathbf{v}_1$ has a valence of N, vertices $\mathbf{v}_2$, $\mathbf{v}_{N+1}$ have valence 6.

as

$$\mathbf{t}_j = \frac{\partial S(\xi_1,\xi_2)}{\partial \xi_j} = \sum_{i=1}^{12} \frac{\partial N_i(\xi_1,\xi_2)}{\partial \xi_j}\mathbf{v}_i,\ j = 1,2, \quad (4)$$

with similar expressions for irregular vertices. A vector basis may therefore be constructed in the tangent space of S as

$$\mathbf{f}(\xi_1,\xi_2) = f_1(\xi_1,\xi_2)\mathbf{t}_1 + f_2(\xi_1,\xi_2)\mathbf{t}_2 \quad (5)$$

This construction allows any higher-order basis set to be directly used on subdivision surfaces. In this work, a pth order Graglia-Wilton-Peterson (GWP) [4] basis is used, although any appropriately behaved (e.g. div-conforming) set may be constructed. The Jacobian of the surface, required for integration, is

$$J(\xi_1,\xi_2) = ||\mathbf{t}_1(\xi_1,\xi_2) \times \mathbf{t}_2(\xi_1,\xi_2)|| \quad (6)$$

and the unit normal is defined as $(\mathbf{t}_1 \times \mathbf{t}_2)/J$.

IV. Results

All results are obtained by solving the Combined Field Integral Equation (CFIE). The first result in fig. 3 is scattered farfield from the $.7\lambda$ sphere in fig. 1 illuminated by an x-polarized plane wave traveling in the $+z$ direction. A $p = 2$ GWP basis is defined on the primal mesh and projected onto the limit surface. Good agreement with the analytical solution is evident.

The second result, scattering from a $3\lambda \times 3\lambda$ Chmutov surface, shows the ease with which subdivision can produce higher order surfaces from topologically nontrivial primal meshes. Fig. 4 shows the $k = 1$ mesh and limit surface for the Chmutov, as well as the incident plane wave. Fig. 5 shows the RCS compared with a reference GWP CFIE implementation and surface currents for a $p = 1$ GWP discretization.

Finally, we show scattering from a 2λ torus that has been deformed by twisting. Figure 6 shows the $k = 1$ mesh for the original torus and the smooth subdivision representation of the twisted mesh, as well as the incident wave direction. RCS and surface currents are shown in fig. 7 for a $p = 1$ GWP discretization.

Acknowledgment: This work was supported by NSF CCF-1018516, NSF CMMI-1250261, and the Department of Defense High Performance Computing Modernization Program Office.

References

[1] F. Cirak, M. Ortiz, and P. Schroder, "Subdivision surfaces: a new paradigm for thin-shell finite-element analysis," *International Journal for Numerical Methods in Engineering*, vol. 47, no. 12, pp. 2039–2072, 2000.

[2] C. Loop, "Smooth subdivision surfaces based on triangles," Department of Mathematics, University of Utah, Aug. 1987.

[3] J. Stam, "Evaluation of loop subdivision surfaces," *Proceedings CD of SIGGRAPH*, vol. 98, 1998.

[4] R. Graglia, D. Wilton, and A. Peterson, "Higher order interpolatory vector bases for computational electromagnetics," *Antennas and Propagation, IEEE Trans. on*, vol. 45, no. 3, pp. 329 –342, 1997.

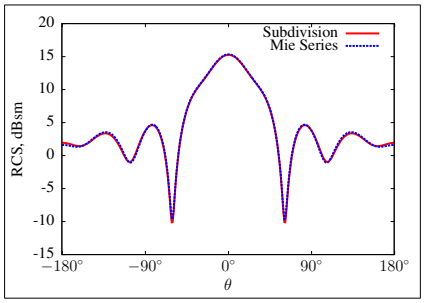

Fig. 3: RCS for $.7\lambda$ subdivision sphere ($\phi = 0°$).

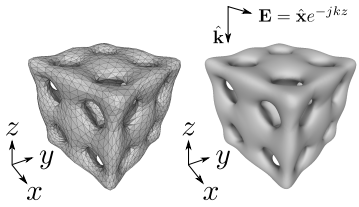

Fig. 4: (a) $k = 1$ Chmutov mesh. (b) Limit surface.

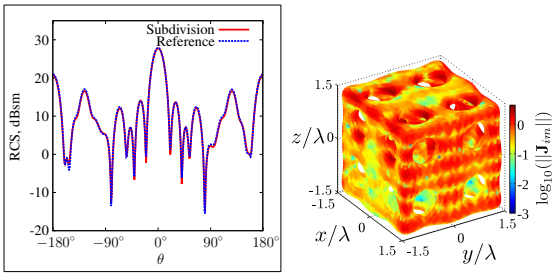

Fig. 5: (a) RCS ($\phi = 0°$) and (b) surface currents for Chmutov surface.

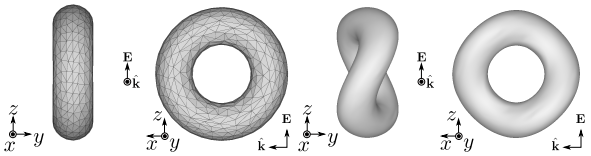

Fig. 6: Torus and deformed torus geometries. (a) Torus mesh (front view) , (b) torus mesh (side view), (c) twisted torus limit surface (front view), (d) twisted torus limit surface (side view).

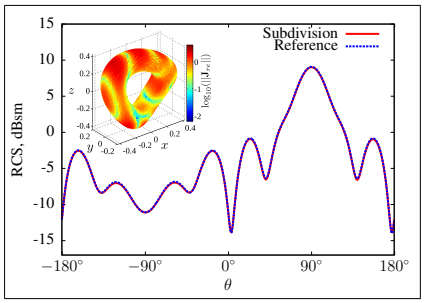

Fig. 7: Twisted torus RCS and surface currents ($\phi = 0°$).